JOURNAL OF SPACECRAFT AND ROCKETS
Vol. 47, No. 6, November–December 2010

Robust Optimization of Thermal–Dynamic Coupling Systems Using a Kriging Model

Lijia Fan,* Zhihai Xiang,† Mingde Xue,‡ and Zhangzhi Cen§
Tsinghua University, 100084 Beijing, People's Republic of China

DOI: 10.2514/1.49307

Thermally induced vibration of the flexible appendages of large-scale space structures may cause adverse effects to astronautical activities. This kind of unexpected response could be controlled to an admissible level through some optimal design methods. Because uncertainties in material properties and structural dimensions are inevitable in practice, they should also be considered during the optimization process to ensure the robust performance of the resultant structure. However, traditional robust design schemes based on either a direct Monte Carlo method or a perturbation-based stochastic finite element method are usually too time-consuming to accomplish this task, because highly nonlinear analysis needs to be repeatedly conducted for this transient problem during the optimization process. To solve this problem, a robust optimization scheme based on the kriging model is developed in this paper. Because of the kriging approximation, only a few thermal–dynamic coupling analyses are needed to construct a satisfactory approximation function of the structural response. Based on this function, the mean value and the standard deviation of the structural response can be obtained efficiently, which greatly facilitates the calculation of the Pareto front for this kind of robust optimal design.

Nomenclature

${}^{t+\Delta t}\ddot{\boldsymbol{a}}$	=	acceleration vector at time $t + \Delta t$
${}^{t+\Delta t}\dot{\boldsymbol{a}}$	=	velocity vector at time $t + \Delta t$
$\boldsymbol{C}$	=	thermal capacity matrix
C_y, C_z	=	coordinates of the shear center relative to the centroid
c	=	specific heat
$\boldsymbol{D}$	=	Rayleigh damping matrix
$\boldsymbol{d}$, $\boldsymbol{d}^-$, $\boldsymbol{d}^+$	=	design variable vector and its lower and upper bounds
E	=	Young's modulus
$f(\boldsymbol{d})$	=	structural response
$\boldsymbol{f}(\boldsymbol{x})$	=	the polynomial regression terms
G	=	shear modulus
k_s	=	thermal conductivities along the circumferential direction
k_x	=	thermal conductivities along the axial direction
$\boldsymbol{K}^m$	=	conduction matrix corresponding to the mth perturbation temperature
${}^t\boldsymbol{K}$	=	stiffness matrix at time t
$\boldsymbol{K}^0$	=	conduction matrix corresponding to the average temperature
$\boldsymbol{M}$	=	mass matrix
N	=	number of design variables
N_p	=	number of Pareto solutions
N_S	=	number of sampling points
$\boldsymbol{P}^m$	=	heat load vector corresponding to the mth perturbation temperature
$\boldsymbol{P}^0$	=	heat load vector corresponding to the average temperature
${}^t\boldsymbol{Q}({}^t\boldsymbol{a})$	=	nodal force vector at time t
q	=	incident heat flux
$\boldsymbol{q}$	=	incident heat flux vector
$\boldsymbol{R}^m(\boldsymbol{T}^0)$	=	radiation matrix
$\boldsymbol{R}^0(\boldsymbol{T}^0)$	=	radiation vector
${}^{t+\Delta t}\Re$	=	total external virtual work at time $t + \Delta t$
${}^{t+\Delta t}\boldsymbol{R}$	=	externally applied nodal load vector at time $t + \Delta t$
${}^t_0\bar{\boldsymbol{R}}$	=	transformation matrix at time t
$\boldsymbol{S}$	=	sampling point matrix
T	=	structural temperature
T_∞	=	ambient temperature
$\boldsymbol{T}^0$	=	average temperature vector
$\boldsymbol{T}^m$	=	mth perturbation temperature vector
t	=	time
${}_tu$	=	incremental displacement at the centroid in x direction
${}^{t+\Delta t}_t\ddot{u}$	=	acceleration in x direction at time $t + \Delta t$ measured in the configuration at time t
${}_tv$	=	incremental displacements at the centroid in y direction
${}^{t+\Delta t}_t\ddot{v}$	=	acceleration in y direction at time $t + \Delta t$ measured in the configuration at time t
${}_tw$	=	incremental displacements at the centroid in z direction
${}^{t+\Delta t}_t\ddot{w}$	=	acceleration in z direction at time $t + \Delta t$ measured in the configuration at time t
$\boldsymbol{x}$	=	variable vector
$\hat{y}(\boldsymbol{x})$	=	response value corresponding to variable vector $\boldsymbol{x}$
$\boldsymbol{y}_s$	=	response vector at sampling points
$Z(\boldsymbol{x})$	=	realization of a stochastic process with zero mean
α	=	thermal expansion coefficient
α_s	=	absorptivity of beam surface
$\boldsymbol{\beta}$	=	coefficients of polynomial regression terms
ε_s	=	emissivity of beam surface
ε_{err}	=	relative error
${}_t\theta_x$	=	incremental rotational angle at the centroid along the x direction
ρ	=	mass density
σ	=	Stefan–Boltzmann constant
σ^2	=	variance of a stochastic process
ω	=	cross-sectional warping function

Subscript

$,x_i$	=	first-order partial derivatives with respect to parameter x_i

Received 10 February 2010; revision received 27 May 2010; accepted for publication 22 June 2010.

*Ph.D. Student, Applied Mechanics Laboratory, Department of Engineering Mechanics; fanlj05@mails.tsinghua.edu.cn.

†Associate Professor, Applied Mechanics Laboratory, Department of Engineering Mechanics; xiangzhihai@tsinghua.edu.cn.

‡Professor, Applied Mechanics Laboratory, Department of Engineering Mechanics; xuemd@mail.tsinghua.edu.cn.

§Professor, Applied Mechanics Laboratory, Department of Engineering Mechanics; demczz@mail.tsinghua.edu.cn.

Superscripts

p	=	incremental displacements of an arbitrary point P
T	=	transpose of a matrix or vector
$*$	=	incremental displacements at the shear center

I. Introduction

DURING the orbital eclipse transition, the flexible appendages of large-scale space structures (LSSSs), which are usually made of thin-walled trusses, are subjected to suddenly applied solar heat flux. This kind of thermal loading is apt to introduce vibration on these structures. Since the 1960s, this unexpected thermally induced vibration has been problematic for several spacecraft [1–3]. A famous event occurred with the Hubble Space Telescope (HST), which experienced an unstable vibration induced by the rapid thermal flux change on the solar array when it passed through a night–day orbital transition. In this phenomenon, the thermal loading is nonlinearly coupled with the dynamic behaviors of structures, which poses a significant engineering challenge to designers. However, this phenomenon was first predicted by Boley [4] before it actually happened. Then Augusti [5] studied radiantly heated rigid links with elastic springs and demonstrated for the first time that unstable thermally induced torsional oscillation is possible. After the problem with the unstable thermally induced vibration of the HST, some researchers showed much interest in this phenomenon. Thornton and Kim [3] analyzed the thermally induced vibration of deployable space structures of the HST by a simplified beam model. Xue and Ding [6] and Xue et al. [7] proposed a Fourier finite element for the transient thermal analysis of thin-walled structures considering heat radiation. In their work, the temperature of the beam cross section is decomposed into the average temperature and perturbation temperatures distributed in the circumferential direction. Because of the orthogonality of the shape functions, these two kinds of temperatures can be decoupled into two equations, which greatly improves the computational efficiency. Based on this Fourier element, Duan et al. [8] gave an explanation of the HST accident by the simulation of the thermally induced vibration of the HST, considering the geometric nonlinearity and thermal–structural coupling effect.

Based on the aforementioned research, it is possible to conduct optimal design to control the harmful thermally induced vibration of LSSSs. However, this is a challenging task, because the high nonlinearities due to radiation, the flexible structures, and the thermal–structural interaction should all be considered in the transient analysis, which is repeatedly conducted during the optimization process. Moreover, it is generally recognized that uncertainties, such as material properties, geometric dimensions, and boundary conditions, are inevitable at every stage of the life cycle of an LSSS. This means if only the deterministic optimization was applied, the performance of the resultant design could be very sensitive to these uncertainties. Thus, one should also consider the uncertainties during the optimal design to ensure the robust performance of the structure.

The robust optimization that considers not only optimality but also robustness has attracted considerable attentions in practical design activities [9–11]. To consider the robustness, the mean value and the variance of a response are considered in the optimization process. However, conventional robust optimization methods can hardly be applied to control the thermally induced vibration of LSSSs, because the nonlinear and transient analyses mentioned above are extremely expensive computationally either using the direct Monte Carlo simulation (DMCS) or perturbation-based stochastic finite element method (PSFEM). Moreover, it is difficult to ensure the accuracy of the stochastic responses obtained from the PSFEM due to the high nonlinearities. One solution to this problem is to use surrogate models that give explicit approximation between the structural response and the design parameters, which greatly facilitates the calculation of statistics [12,13]. Since the surrogate model is just an approximation, the accuracy of the robust optimization based on the surrogate model largely depends on whether this model can capture the general tendencies of the design behavior and how accurate it is in capturing the performance variations. After some years of comparison, researchers recognize that the kriging approximation has better performance than other surrogate models, such as polynomial or radial basis function, when robustness is taken into account [14–16]. Jin et al. [17] have shown that kriging is superior to other two methods through a simple two-bar robust design problem. The main reason is that the kriging model is a stochastic process [18], which can adapt well to nonlinear function. In addition, the kriging model gives not only estimated function values but also approximation errors, which help to determine locations in the design space where additional points of response data should be considered for improving the model accuracy. Based on the above two reasons, the kriging model is adopted to give explicit approximation of the thermal–dynamic coupling systems in this study.

In this paper, a robust design scheme based on the kriging model is developed to control the thermally induced vibration of LSSSs. In this scheme, an adaptive space estimation process is constructed according to the kriging approximation to replace the expensive thermal–dynamic coupling reanalysis. Based on the resultant approximation function, the Monte Carlo simulation (MCS) and PSFEM could be applied to obtain the stochastic structural responses. Then the objective function that involves the mean value and the standard deviation (Std) of structural responses is formulated for the robust design of LSSS. Finally, the Pareto-optimal solutions are obtained to suggest a proper design.

II. Thermal–Dynamic Coupling Analysis of LSSS Considering Geometric Nonlinearity

To make the background of this research more clear, this section gives a brief introduction of the thermal–dynamic coupling analysis of flexible LSSS [8]. As Fig. 1 shows, the flexible appendages of LSSSs are usually made of thin-walled closed or open beams, which are subjected to alternate solar heat flux while emitting thermal energy to space by radiation. In the following deduction, a local Cartesian coordinate system (x, y, z) is attached at the centroid O of the thin-walled beam element, where the x axis coincides with the centroidal line, and the y and z axes are the principal axes of the section. The circumferential coordinate along the midline of the cross section is denoted as s, which ranges from zero to S_h, the perimeter of the midline. For the thin-walled beam, it is assumed that $t_s \ll S_h \ll l$; thus, the temperature gradient along the beam thickness can be ignored. In the following analysis, thermal energy is emitted from the external beam surface, but internal radiation within the beam is neglected [3,7].

A. Transient Temperature Analysis of Thin-Walled Beams

The temperature $T(s, x, t)$ of the thin-walled beam element should satisfy a nonlinear partial differential equation [6,7] as

$$c\rho\frac{\partial T}{\partial t} - \frac{\partial}{\partial x}\left(k_x\frac{\partial T}{\partial x}\right) - \frac{\partial}{\partial s}\left(k_s\frac{\partial T}{\partial s}\right) + \frac{\varepsilon\sigma}{t_s}(T^4 - T_\infty^4) - \frac{\alpha_s}{t_s}q(s, x, t) = 0 \tag{1}$$

The temperature in the cross section can be separated into average and perturbation parts and is interpolated by the values at two element nodes:

$$T(s, x, t) \approx \sum_{i=1}^{2}\left[T_i^0(t) + \sum_{m=1}^{M} T_i^m(t)N^m(s)\right]N_i(x) \tag{2}$$

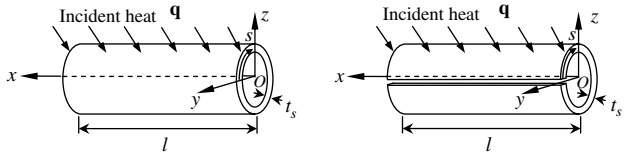

a) Closed section **b) Open section**

Fig. 1 Thin-walled beam elements.

where i is the node number, $T_i^0(t)$ is the average temperature, and $T_i^m(t)$ is the perturbation temperature along the circumferential direction on the beam cross section; $N_i(x)$ is the linear interpolating function along the length of this two-node beam element; and $N^m(s)$ is the shape function along the circumference of the beam cross section. Because of the orthogonality between $N_i(x)$ and $N^m(s)$, the heat conduction equations can be decoupled into the following two sets, and so the perturbation temperature can be solved after obtaining the average temperature:

$$\boldsymbol{C}\,\dot{\boldsymbol{T}}^0 + \boldsymbol{K}^0\boldsymbol{T}^0 + \boldsymbol{R}^0(\boldsymbol{T}^0) = \boldsymbol{P}^0(t) \tag{3}$$

$$\boldsymbol{C}\,\dot{\boldsymbol{T}}^m + [\boldsymbol{K}^m + \boldsymbol{R}^m(\boldsymbol{T}^0)]\boldsymbol{T}^m = \boldsymbol{P}^m(t) \tag{4}$$

The details can be found in [6,7].

B. Thermal–Dynamic Coupling Formulations Considering Geometric Nonlinearity

During the orbital day–night crossing period, the suddenly applied heat flux is apt to introduce vibrations on LSSSs. The heat flux quickly increases (in a nearly step-function fashion) and enters the sunlit side of the beam at an angle α, causing thermal expansion of that side. The resulting bending away from the sunward direction reduces the angle α. That reduction diminishes the heat flux absorbed by the beam and correspondingly decreases the thermal expansion, thus enabling the elastic resistance to move the beam back toward the sun, which restores α and the absorbed heat flux, and the cycle repeats. Given the structural damping and the angle α tending to 90 deg as the structure moves into the sunlit side of the orbit, the cycle amplitude is damped out and the steady state prevails. To formulate the aforementioned thermal–structural coupling phenomenon, one has to construct the structural dynamic equation that contains the thermal loading, which is also dependent on the deformation of the structure. Besides this nonlinearity of boundary conditions, the geometric nonlinearity should also be considered for these flexible structures.

It is assumed that strains are sufficiently small so that the sectional properties (areas and inertias) remain unchanged during the large deformation and rotation of this Euler–Bernoulli beam. As Fig. 2 shows, the element local coordinate system changes along with the rigid movements of the element. From time t to $t+\Delta t$, the incremental displacements of an arbitrary point P on the cross section of the beam can be expressed as

$$
\begin{aligned}
{}_tu^p &= {}_tu - y\frac{\partial_t v^*}{\partial x} - z\frac{\partial_t w^*}{\partial x} - \omega\frac{\partial_t \theta_x}{\partial x} \qquad {}_tv^p = {}_tv^* - (z-C_z)_t\theta_x \\
{}_tw^p &= {}_tw^* + (y-C_y)_t\theta_x
\end{aligned} \tag{5}
$$

The principle of virtual displacement established at time $t+\Delta t$ can be written as

$$
\begin{aligned}
&\int_0^l \iint_A ({}_t^{t+\Delta t}\sigma_{xx}\delta_t\varepsilon_{xx} + {}_t^{t+\Delta t}\sigma_{xy}\delta_t\gamma_{xy} + {}_t^{t+\Delta t}\sigma_{xz}\delta_t\gamma_{xz})\mathrm{d}y\,\mathrm{d}z\,\mathrm{d}x \\
&\quad = {}^{t+\Delta t}\Re - \int_0^l \iint_A \rho({}_t^{t+\Delta t}\ddot{u}\delta_t u + {}_t^{t+\Delta t}\ddot{v}\delta_t v + {}_t^{t+\Delta t}\ddot{w}\delta_t w)\mathrm{d}y\,\mathrm{d}z\,\mathrm{d}x
\end{aligned} \tag{6}
$$

where the incremental strains can be calculated as

$$
\begin{aligned}
{}_t\varepsilon_{xx} &= \frac{\partial_t u^p}{\partial x} + \frac{1}{2}\left[\left(\frac{\partial_t u^p}{\partial x}\right)^2 + \left(\frac{\partial_t v^p}{\partial x}\right)^2 + \left(\frac{\partial_t w^p}{\partial x}\right)^2\right] \\
{}_t\gamma_{xy} &= \frac{\partial_t u^p}{\partial y} + \frac{\partial_t v^p}{\partial x} + \frac{\partial_t u^p}{\partial x}\frac{\partial_t u^p}{\partial y} + \frac{\partial_t v^p}{\partial x}\frac{\partial_t v^p}{\partial y} + \frac{\partial_t w^p}{\partial x}\frac{\partial_t w^p}{\partial y} \\
{}_t\gamma_{xz} &= \frac{\partial_t u^p}{\partial z} + \frac{\partial_t w^p}{\partial x} + \frac{\partial_t u^p}{\partial x}\frac{\partial_t u^p}{\partial z} + \frac{\partial_t v^p}{\partial x}\frac{\partial_t v^p}{\partial z} + \frac{\partial_t w^p}{\partial x}\frac{\partial_t w^p}{\partial z}
\end{aligned} \tag{7}
$$

and the stresses at time $t+\Delta t$ measured in the configuration at time t are

$$
\begin{aligned}
{}_t^{t+\Delta t}\sigma_{xx} &= {}^t\tau_{xx} + E[{}_t\varepsilon_{xx} - \alpha({}^{t+\Delta t}T - {}^tT)] \\
{}_t^{t+\Delta t}\sigma_{xy} &= {}^t\tau_{xy} + G_t\gamma_{xy} \qquad {}_t^{t+\Delta t}\sigma_{xz} = {}^t\tau_{xz} + G_t\gamma_{xz}
\end{aligned} \tag{8}
$$

where ${}^t\tau_{xx}$, ${}^t\tau_{xy}$, and ${}^t\tau_{xz}$ are Cauchy stresses at time t, and ${}^tT$ and ${}^{t+\Delta t}T$ are the temperatures at time t and $t+\Delta t$, respectively.

Substituting Eqs. (7) and (8) into Eq. (6) and transforming into the global Cartesian coordinate system, one obtains

$$\boldsymbol{M}\,{}^{t+\Delta t}\ddot{\boldsymbol{a}} + \boldsymbol{D}^{t+\Delta t}\dot{\boldsymbol{a}} + {}^t\boldsymbol{K}({}^t\boldsymbol{a})\Delta\boldsymbol{a} = {}^{t+\Delta t}\boldsymbol{R} - {}^t\boldsymbol{Q}({}^t\boldsymbol{a}) \tag{9}$$

where $\Delta\boldsymbol{a}$ is the incremental displacement vector.

When a beam is subjected to a suddenly applied heat flux, this thermal loading may induce structural vibrations according to Eq. (9). Meanwhile, the incident heat flux measured in the local

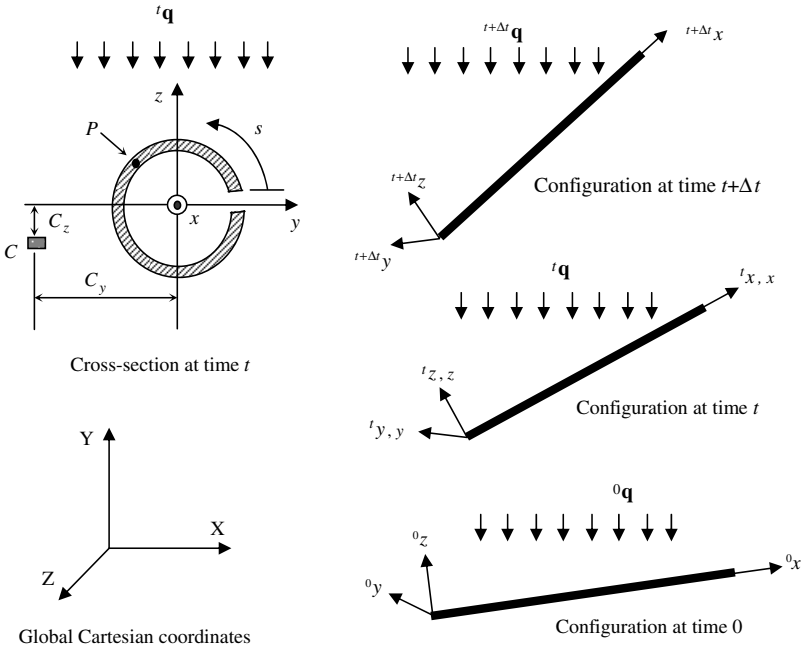

Fig. 2 Motion of the thin-walled beam element.

coordinate system changes with the deformation of the beam (see Fig. 2). This change can be described by the transformation matrix ${}^t_0\bar{\boldsymbol{R}}$ as follows:

$$ {}^t_t\boldsymbol{q} = {}^t_0\bar{\boldsymbol{R}}\,{}^t_0\boldsymbol{q} \tag{10} $$

where ${}^t_t\boldsymbol{q}$ and ${}^t_0\boldsymbol{q}$ are incident heat fluxes measured in the current and original coordinate systems, respectively. Therefore, Eqs. (3) and (4) can be expressed as

$$ \boldsymbol{C}\,\dot{\boldsymbol{T}}^0 + \boldsymbol{K}^0\boldsymbol{T}^0 + \boldsymbol{R}^0(\boldsymbol{T}^0) = \boldsymbol{P}^0({}^t_0\boldsymbol{q}, {}^t\boldsymbol{a}) \tag{11} $$

$$ \boldsymbol{C}\,\dot{\boldsymbol{T}}^m + [\boldsymbol{K}^m + \boldsymbol{R}^m(\boldsymbol{T}^0)]\boldsymbol{T}^m = \boldsymbol{P}^m({}^t_0\boldsymbol{q}, {}^t\boldsymbol{a}) \tag{12} $$

The detailed expressions of the above matrices and vectors can be found in [8].

For the thermal–structural coupling analysis, the transient temperature is solved from Eqs. (11) and (12) first, then dynamic deformations due to the thermal load are obtained from Eq. (9). According to these deformations, the updated ${}^t_0\bar{\boldsymbol{R}}$ can be substituted back into Eqs. (11) and (12) and obtains the updated temperature. This process continues until the calculated temperature converges to a constant value.

III. Kriging Model

As Sec. II illustrates, the thermal–dynamic coupling analysis of LSSSs involves some high nonlinearities, and so it is a complicated and time-consuming process. Instead of repeatedly conducting such expensive computation as required by the optimal design of structures, one can use a surrogate model that uses a simple function to approximate the relation between structural responses and design parameters. For this purpose, the kriging method is adopted. It was originally developed in geostatistics by a South African mining engineer named Krige and was applied in the field of deterministic simulation for the design and analysis of computer experiments by Sacks et al. [18].

The kriging method adopts the model that treats the deterministic response $y(\boldsymbol{x})$ as a realization of a stochastic process that can be expressed in a regression model:

$$ y(\boldsymbol{x}) = \boldsymbol{f}^T(\boldsymbol{x})\boldsymbol{\beta} + Z(\boldsymbol{x}) \tag{13} $$

where $\boldsymbol{f}(\boldsymbol{x})$ is a given polynomial regression of input $\boldsymbol{x}$, and $Z(\boldsymbol{x})$ is a stochastic process that is assumed to have mean zero and covariance

$$ \mathrm{Cov}\,[Z(\boldsymbol{x}^i), Z(\boldsymbol{x}^j)] = \sigma^2 R(\boldsymbol{x}^i, \boldsymbol{x}^j) \tag{14} $$

where superscripts i and j indicate the ith and jth sampling points, respectively; σ^2 is the process variance; and$R(\boldsymbol{x}^i, \boldsymbol{x}^j)$ is the correlation. It requires $R(\boldsymbol{x}^i, \boldsymbol{x}^j)$ to be smooth enough to obtain the analytic derivative of response $y(\boldsymbol{x})$ over $\boldsymbol{x}$, which is used in PSFEM (see Sec. IV) and the gradient-based optimization method (see Sec. V). For this purpose, it is convenient to take the Gaussian form of

$$ R(\boldsymbol{x}^i, \boldsymbol{x}^j) = \prod_{l=1}^{N} \exp[-\theta_l (x_l^i - x_l^j)^2] $$

where θ_l are the coefficients corresponding to the lth item of $\boldsymbol{x}$.

Using responses $\boldsymbol{y}_s = \{y^1, \ldots, y^{N_S}\}$ at given sampling points $\boldsymbol{S} = \{\boldsymbol{x}^1, \ldots, \boldsymbol{x}^{N_S}\}$, the kriging method considers a linear predictor $\hat{y}(\boldsymbol{x}) = \boldsymbol{c}^T(\boldsymbol{x})\boldsymbol{y}_S$ of $y(\boldsymbol{x})$ at untried point $\boldsymbol{x}$. The mean squared error (MSE) of this predictor averaged over the stochastic process should be minimized, since the kriging model is the best linear unbiased predictor. In this way, one can obtain the estimated value of $\boldsymbol{\beta}$, denoted by $\hat{\boldsymbol{\beta}}$ and Eq. (13) becomes

$$ \hat{y}(\boldsymbol{x}) = \boldsymbol{f}^T(\boldsymbol{x})\hat{\boldsymbol{\beta}} + \boldsymbol{r}^T(\boldsymbol{x})\boldsymbol{R}^{-1}(\boldsymbol{y}_S - \boldsymbol{F}\hat{\boldsymbol{\beta}}) \tag{15} $$

where $\boldsymbol{R}$ is the correlation matrix of given sampling points, $\boldsymbol{r}(\boldsymbol{x})$ is the vector of correlations between the given sampling points and $\boldsymbol{x}$:

$$ \boldsymbol{r}(\boldsymbol{x}) = [R(\boldsymbol{x}^1, \boldsymbol{x}), \ldots, R(\boldsymbol{x}^{N_S}, \boldsymbol{x})]^T \tag{16} $$

and

$$ \boldsymbol{F} = [\boldsymbol{f}(\boldsymbol{x}^1), \ldots, \boldsymbol{f}(\boldsymbol{x}^{N_S})]^T \tag{17} $$

Define the likelihood function L as

$$ L(\boldsymbol{y}, \boldsymbol{\theta}, \boldsymbol{\beta}, \sigma^2) = \frac{(2\pi\sigma^2)^{-N_S/2}}{\sqrt{|\boldsymbol{R}|}} \exp\left[-\frac{(\boldsymbol{y} - \boldsymbol{F}\boldsymbol{\beta})^T \boldsymbol{R}^{-1}(\boldsymbol{y} - \boldsymbol{F}\boldsymbol{\beta})}{2\sigma^2}\right] \tag{18} $$

where $\boldsymbol{\theta} = (\theta_1, \ldots, \theta_N)^T$. The maximum likelihood estimations of $\boldsymbol{\beta}$ and σ^2 are

$$ \hat{\boldsymbol{\beta}} = (\boldsymbol{F}^T\boldsymbol{R}^{-1}\boldsymbol{F})^{-1}\boldsymbol{F}^T\boldsymbol{R}^{-1}\boldsymbol{y}_S \tag{19} $$

$$ \hat{\sigma}^2 = \frac{(\boldsymbol{y}_S - \boldsymbol{F}\boldsymbol{\beta})^T \boldsymbol{R}^{-1}(\boldsymbol{y}_S - \boldsymbol{F}\boldsymbol{\beta})}{N_S} \tag{20} $$

Similarly, the maximum likelihood estimation of $\boldsymbol{\theta}$ can be obtained by

$$ \hat{\boldsymbol{\theta}} = \mathrm{minimize}\{(|\boldsymbol{R}|)^{1/N_S}\hat{\sigma}^2\} \tag{21} $$

The kriging model gives not only the estimated function value but also the MSE, which helps to determine the locations in the design space where additional points of response data should be considered to improve the approximation. A convenient representation of the MSE is

$$ \mathrm{MSE}\,[\hat{y}(\boldsymbol{x})] = \hat{\sigma}^2\left[1 - (\boldsymbol{f}^T(\boldsymbol{x}), \boldsymbol{r}^T(\boldsymbol{x}))\begin{pmatrix} 0 & \boldsymbol{F}^T \\ \boldsymbol{F} & \boldsymbol{R} \end{pmatrix}^{-1}\begin{pmatrix} \boldsymbol{f}(\boldsymbol{x}) \\ \boldsymbol{r}(\boldsymbol{x}) \end{pmatrix}\right] \tag{22} $$

According to Eq. (22), one can define a relative error at point $\boldsymbol{x}$:

$$ \varepsilon_{\mathrm{err}}(\boldsymbol{x}) = \frac{\sqrt{\mathrm{MSE}[\hat{y}(\boldsymbol{x})]}}{|\hat{y}(\boldsymbol{x})|} \tag{23} $$

The performance of the kriging model strongly depends on the sampling point's location and density. However, the number of sampling points should be kept as small as possible to reduce the computational cost on account of the expensive high nonlinear computation of the thermally induced responses at sampling points. For this purpose, two initial sampling-point selection algorithms are adopted in this paper. One is the rectangular grid (RG) method that just uses a uniform rectangular grid to cover the design space. Another is the translational propagation algorithm that creates Latin hypercube designs (TPLHD) [19]. After obtaining the initial sampling points, an adaptive kriging model process can be constructed as follows:

1) Calculate the true function values $\boldsymbol{y}_s$ at initial sampling points.

2) Generate the kriging model using Eq. (15).

3) Calculate the relative error $\varepsilon_{\mathrm{err}}$ using Eq. (23) at N_{test} testing points. Because the location of the $(\varepsilon_{\mathrm{err}})_{\max}$ cannot be given directly,

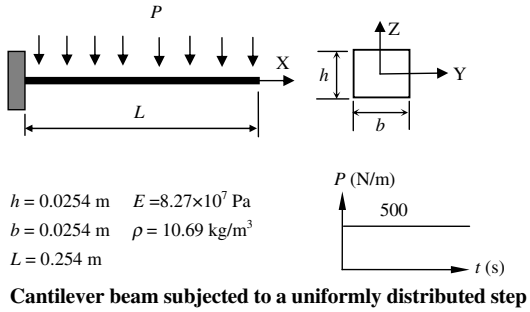

Fig. 3 Cantilever beam subjected to a uniformly distributed step load.

Table 1 CVs of random variables

	CV		
Random variable	Case 1	Case 2	Case 3
b	0.05	0.10	0.25
h	0.05	0.10	0.25
E	0.05	0.10	0.40

the testing points should cover the whole design space with high density, which is enough to find the location of the maximal or near maximal error. The RG is adopted here, which can meet all these demands mentioned above and is suitable to be applied to obtain the test points.

4) If $(\varepsilon_{\text{err}})_{\max}$ is less than a prescribed tolerance, stop; otherwise, calculate the true function value at the point with the maximum relative error, and add this new sampling point to the original sampling points, go to step 2.

IV. Stochastic Analysis of LSSS

From Eq. (15) one can find that $\hat{y}(\boldsymbol{x})$ is a very simple and explicit function, and so the popular PSFEM [20], which is a nonstatistical method that only requires the mean value and variances of the random variables, can be easily employed to obtain the mean value and the variance of the structural response. Based on perturbation method, the stochastic version of $\hat{y}(\boldsymbol{x})$ can be obtained through Taylor expansion about the mean value of random variables up to the first-order term. Subsequently, the mean value $\mathrm{E}[\hat{y}(\boldsymbol{x})]$ and the variance $\mathrm{Var}[\hat{y}(\boldsymbol{x})]$ are obtained as

$$\mathrm{E}\,[\hat{y}(\boldsymbol{x})] \approx \bar{\hat{y}} = \hat{y}(\bar{\boldsymbol{x}}) \tag{24}$$

$$\mathrm{Var}\,[\hat{y}(\boldsymbol{x})] \approx \sum_{i,j=1}^{N} \bar{\hat{y}}_{,x_i} \bar{\hat{y}}_{,x_j} \mathrm{Cov}(x_i, x_j) \tag{25}$$

where the upper bar indicates that the corresponding quantity is evaluated at the mean values of the random parameters. Differentiating $\hat{y}(\boldsymbol{x})$ with respect to parameter $\boldsymbol{x}$, the first derivation of $\hat{y}(\boldsymbol{x})$ can be obtained:

$$\frac{\partial \hat{y}(\boldsymbol{x})}{\partial \boldsymbol{x}} = \boldsymbol{J}_{\boldsymbol{f}}^{T} \hat{\boldsymbol{\beta}} + \boldsymbol{J}_{\boldsymbol{r}}^{T} \boldsymbol{R}^{-1} (\boldsymbol{y}_s - \boldsymbol{F}\hat{\boldsymbol{\beta}}) \tag{26}$$

where $(\boldsymbol{J}_{\boldsymbol{f}})_{ij} = \partial f_i / \partial x_j$ and $(\boldsymbol{J}_{\boldsymbol{r}})_{ij} = \partial r_i / \partial x_j$.

It is well known that the PSFEM is only valid for the problem with a small ratio of standard deviation over the mean value, called the coefficient of variation (CV) [20]. To overcome this limitation, one can use the MCS to solve the problem with large CV, since Eq. (15) can be efficiently evaluated. However, because the implementation of the MCS is limited to the known distribution functions of the random variables, one should compromise between these two methods according to the practical condition.

V. Robust Optimization of LSSS

The robust optimization tries to optimize the structural performance while ensuring its insensitivity to small changes of the structural parameters. This is achieved by minimizing both the mean value and the Std of the structural performance function simultaneously, which can be formulated as a biobjective optimization problem:

$$\begin{aligned} &\text{find} \quad \boldsymbol{d} \\ &\text{minimize} \quad \mathrm{E}[f(\boldsymbol{d})] \quad \text{and} \quad \mathrm{Std}[f(\boldsymbol{d})] \\ &\text{subject to} \quad \boldsymbol{d}^{-} + \boldsymbol{\delta} \le \boldsymbol{d} \le \boldsymbol{d}^{+} - \boldsymbol{\delta} \end{aligned} \tag{27}$$

where $\boldsymbol{\delta}$ can be regarded as the variation of design variables.

Because the two objectives in Eq. (27) often conflict with each other and the mean value will decrease along with the increment of the Std, a tradeoff decision is needed to choose the best design from the Pareto front in objective space. To obtain the Pareto front, this paper just uses a very simple method that translates Eq. (27) into a single-objective optimization problem by adding an equality constraint. First, the single-objective optimization problems with the mean value and the Std are solved independently to obtain the optimal solutions $\boldsymbol{d}^{1^*}$ and $\boldsymbol{d}^{2^*}$, respectively. Then the utopia points are defined as

$$\mathrm{E}^{U} = \mathrm{E}[f(\boldsymbol{d}^{1^*})] \tag{28}$$

$$\mathrm{Std}^{U} = \mathrm{Std}[f(\boldsymbol{d}^{2^*})] \tag{29}$$

and the nadir points are defined as

$$\mathrm{E}^{N} = \max\{\mathrm{E}[f(\boldsymbol{d}^{1^*})], \mathrm{E}[f(\boldsymbol{d}^{2^*})]\} \tag{30}$$

$$\mathrm{Std}^{N} = \max\{\mathrm{Std}[f(\boldsymbol{d}^{1^*})], \mathrm{Std}[f(\boldsymbol{d}^{2^*})]\} \tag{31}$$

Choosing the Std as the objective function, Eq. (27) can be rewritten as

$$\begin{aligned} &\text{find} \quad \boldsymbol{d} \\ &\text{minimize} \quad \mathrm{Std}[f(\boldsymbol{d})] \\ &\text{subject to} \quad \mathrm{E}[f(\boldsymbol{d})] = E_i \\ &\quad \boldsymbol{d}^{-} + \boldsymbol{\delta} \le \boldsymbol{d} \le \boldsymbol{d}^{+} - \boldsymbol{\delta} \end{aligned} \tag{32}$$

where $\mathrm{E}_i (i = 1, \ldots, N_p)$ is the given value in $[\mathrm{E}^{U}, \mathrm{E}^{N}]$ by designers. Alternatively, the mean value can also be chosen as the objective function. With this method, one can efficiently obtain the evenly distributed solutions on the Pareto front.

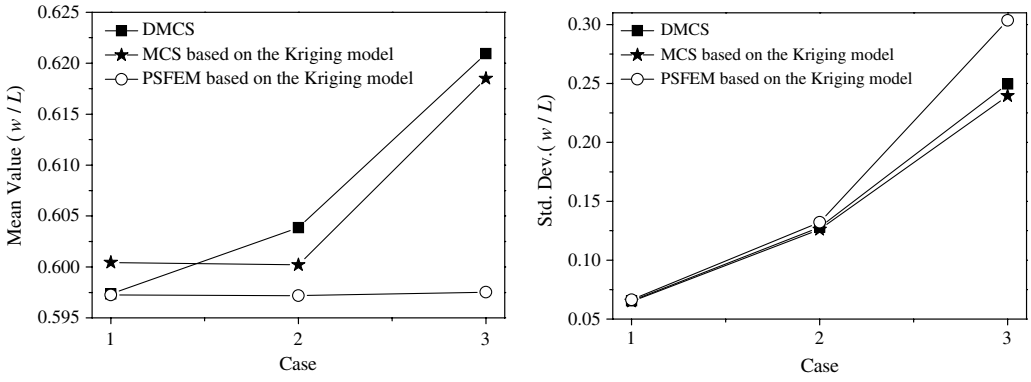

Fig. 4 Mean value and the Std of the tip deflection.

Table 2 Stochastic response of nodal deflection w/L (case 2)

		Kriging model					
		RG (fixed) ($5 \times 4 \times 5$ points)		TPLHD (adaptive) Initial (20 points)		Final (28 points)	
	DMCS	MCS	PSFEM	MCS	PSFEM	MCS	PSFEM
Mean value	0.604	0.600	0.597	0.608	0.598	0.603	0.597
Absolute relative error, %	——	0.662	1.159	0.662	0.993	0.166	1.159
Std	0.128	0.126	0.132	0.125	0.124	0.126	0.134
Absolute relative error, %	——	1.563	3.125	2.344	3.125	1.563	4.688

A vector function $\boldsymbol{F}(\boldsymbol{d})$ is defined as

$$\boldsymbol{F}(\boldsymbol{d}) = \{F_1(\boldsymbol{d}), F_2(\boldsymbol{d}), \ldots, F_M(\boldsymbol{d})\}^T \tag{33}$$

The vector $\boldsymbol{F}(\bar{\boldsymbol{d}})$ is said to dominate another vector $\boldsymbol{F}(\hat{\boldsymbol{d}})$, denoted as $\boldsymbol{F}(\bar{\boldsymbol{d}}) \prec \boldsymbol{F}(\hat{\boldsymbol{d}})$, if and only if $F_i(\bar{\boldsymbol{d}}) \leq F_i(\hat{\boldsymbol{d}})$ for all $i \in \{1, 2, \ldots, M\}$ and $F_j(\bar{\boldsymbol{d}}) < F_j(\hat{\boldsymbol{d}})$ for some $j \in \{1, 2, \ldots, M\}$. A point $\boldsymbol{d}^* \in [\boldsymbol{d}^- + \boldsymbol{\delta}, \boldsymbol{d}^+ - \boldsymbol{\delta}]$ is said to be globally Pareto-optimal or a globally efficient point if and only if there does not exist $\boldsymbol{d} \in [\boldsymbol{d}^- + \boldsymbol{\delta}, \boldsymbol{d}^+ - \boldsymbol{\delta}]$ satisfying $\boldsymbol{F}(\boldsymbol{d}) \prec \boldsymbol{F}(\boldsymbol{d}^*)$.

However, since some non-Pareto solutions may also be found during this process, a Pareto filter, which is used to identify the non-Pareto solutions according to the definition of the Pareto-optimal point, needs to be applied as a postprocessing method.

The suboptimization problem defined by Eq. (32) can be efficiently solved with mathematical programming methods. If the PSFEM is applied, a gradient-based optimization method such as sequential quadratic programming method [21] can be used, because all required sensitivities can be calculated analytically by differentiating Eqs. (24) and (25). If the MCS is used, non-gradient-based methods such as Hooke–Jeeves direct search method [21] can be employed.

VI. Numerical Examples

Two numerical examples are presented in this section to demonstrate the performance of the proposed method. First, the validity of the stochastic response obtained by the kriging method is checked by comparing with the results from the DMCS. Then robust optimizations are applied to other two examples to illustrate the capability of the proposed robust optimization scheme. In all these examples, random variables are assumed to follow uniform distributions, and 1000 samples are used for the DMCS and the MCS based on the kriging model.

A. Cantilever Beam Subjected to a Uniformly Distributed Step Load

Figure 3 shows a cantilever beam subjected to uniformly distributed step load. To obtain the nodal deflections in 0.0135 s, the time step of $\Delta t = 1.35 \times 10^{-4}$ s is adopted in the dynamic analysis considering geometric nonlinearity. The tip deflection is taken as objective function to be minimized.

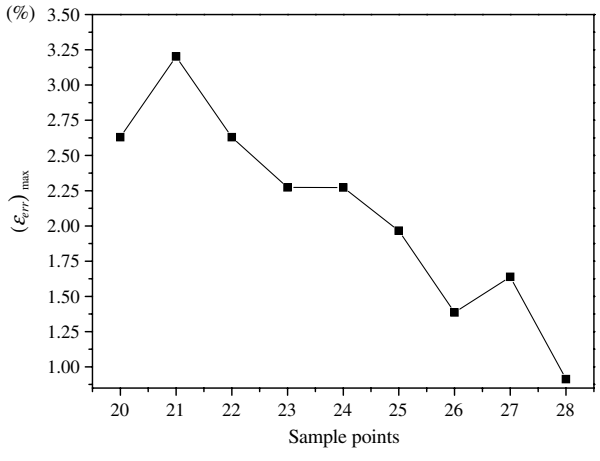

Fig. 5 The $(\varepsilon_{\mathrm{err}})_{\max}$ during the adaptive process (case 2).

1. *Stochastic Analysis of the Cantilever Beam*

The parameters b and h and Young's modulus E are taken as random variables with three cases of different CVs (listed in Table 1).

First, the kriging model is constructed using fixed $5 \times 4 \times 5$ sampling points obtained by RG method. Based on this approximated model, the mean value and the Std of the tip deflection solved by the MCS and PSFEM are compared with the results from the DMCS in Fig. 4. The results obtained by the MCS based on the kriging model are in good agreement with those from the DMCS for all three cases. But the computational errors of the results from the PSFEM increase along with the increment of CV. The errors of case 3 are too large to be acceptable.

Table 2 shows the mean value and the Std of the tip deflection obtained by different sampling methods for case 2. It shows that the results from the approximation methods agree very well with those from the DMCS. The adaptive kriging model that uses 20 initial sampling points by the TPLHD and 28 final sampling points can achieve the same accuracy as the fixed kriging model using $5 \times 4 \times 5$ sampling points by RG method, but with many fewer sampling points. The corresponding $(\varepsilon_{\mathrm{err}})_{\max}$ during the adaptive process is shown in Fig. 5. It reveals that the adaptive process is very efficient for improving the accuracy of the kriging model. In addition, the results from the PSFEM are worse than those from the MCS. This is reasonable, because the PSFEM uses the Taylor expansion to estimate the functions.

The CVs in case 3 are so large that only the results from MCS are listed in Table 3. It shows that the stochastic problem can be solved with good accuracy even with such large CVs. Moreover, the errors of the mean value and the Std can be greatly reduced from the initial 20 sampling points through the adaptive TPLHD process.

Overall, the MCS and the PSFEM based on the kriging model performance very well in solving stochastic problems. But for the problem with large CV, the MCS can get more accurate results than the PSFEM. In addition, the TPLHD method is more favorable to generate the initial sampling points for the multivariable approximation problem, because the initial number of sampling points can be limited by applying the adaptive scheme proposed in Sec. IV.

Table 3 Stochastic response of nodal deflection w/L (case 3)

		Kriging model		
		RG (fixed) ($5 \times 4 \times 5$ points)	TPLHD (adaptive) Initial (20 points)	Final (69 points)
	DMCS	MCS	MCS	MCS
Mean value	0.621	0.619	0.630	0.616
Absolute relative error, %	——	0.322	1.127	0.805
Std	0.250	0.240	0.224	0.250
Absolute relative error, %	——	4.000	10.400	0.000

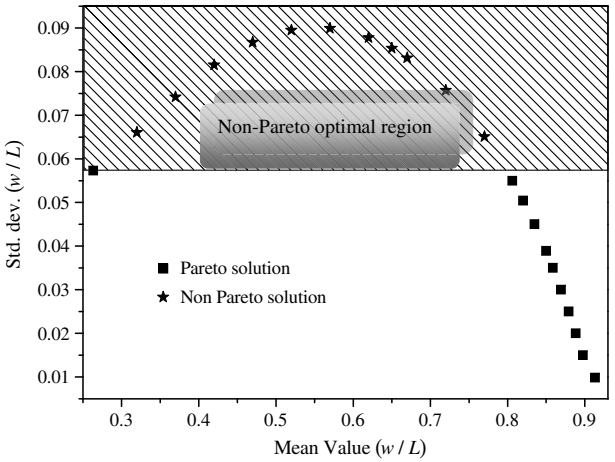

Fig. 6 Pareto front of the tip deflection.

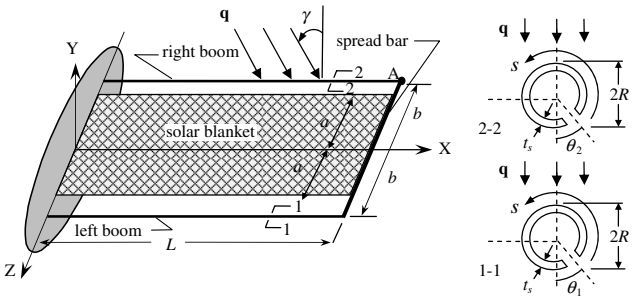

Fig. 7 Model of the HST solar array.

2. Robust Optimization of the Cantilever Beam

The objective in the robust design of this cantilever beam is to minimize the mean value and the Std of the tip deflection by adjusting the two geometric parameters b and h listed in Table 1. These two design variables are in the same interval of [1.462, 3.694]. All three parameters listed in Table 1 are taken as random variables with the CV of 0.07. The PSFEM based on the kriging model is used to calculate the stochastic responses. Therefore, the sequential quadratic programming method [21] is employed to solve this optimization problem since all sensitivities needed can be analytically calculated. After applying the robust optimization mentioned in Sec. V, one can obtain the Pareto front of this problem (shown in Fig. 6) and the corresponding optimal results (listed in Table 4). It should be noted that some non-Pareto solutions are generated, and so a filter (see Sec. V) is used to remove them from the Pareto front according to the definition of the Pareto solution. With this method, one can obtain arbitrary Pareto solutions at the designer's will.

B. HST Solar Array Subjected to Suddenly Applied Solar Heat Flux

The LSSS will probably experience thermally induced vibration due to the sudden temperature changes during the orbital day–night crossing period. The most famous accident is the failure of the HST in 1990. Although some research [3,7,8] has been carried out to explain the occurrence of this phenomenon, it is limited to the deterministic analyses. With the confidence obtained from the previous examples, we try to carry out the robust optimization for the HST solar array in this section.

The model of the HST solar array is shown in Fig. 7. The left and right booms are open thin-walled circular beams formed by spreading and curling thin-walled membranes. Because of the controlling error of the spreading machine, it is very difficult to ensure that the slits of the two booms point in the same direction. Therefore, it is reasonable to assume that the slit of the booms deviate from the Y axis with θ degree (see Fig. 7). The solar blanket is modeled by the beam grids with 29.5 N preapplied tension force. Accordingly, the left and right booms have 14.75 N preapplied tension forces, respectively. The material and geometric parameters can be found in [8]. The suddenly applied 1350 $\mathrm{W/m^2}$ incident heat flux is in the X-Y plane with the incident angle of $\gamma = 60°$. Thermal–dynamic coupling effect and geometric nonlinearity are considered in the analysis of the transient response of this structure. The goal of the robust optimization is to minimize the maximum deflection of point A during the period of 600 s and ensure a stable performance of this structure when some uncertainties are present.

1. Stochastic Analysis of the HST Solar Array

First, two angles (θ_1 and θ_2) are considered as random variables within the interval of [−15°, 15°]. The response surface using 25 initial sampling points (denoted by dark dots) by the RG method is shown in Fig. 8a. After the adaptive process, the final obtained response surface contains 41 sampling points (denoted by dark dots), shown in Fig. 8b. It shows that the response surface is greatly improved through the adaptive process and only 16 additional points are added. Then the TPLHD method is also applied to obtain the initial sampling points to construct another kriging model. Based on these two approximation surfaces, the MCS is employed to calculate the mean value and the Std of the maximum deflection at point A (listed in Table 5). The accuracies of these two kriging models are nearly the same. The computing time of the DMCS on an Intel Core 2–2.4 GHz computer is about 7240 min, while only about 300 min are needed for the MCS based on the kriging models.

Furthermore, the emissivity coefficient ε and the absorptivity coefficient α_s on the external surface of the two booms are also considered as random variables with the CV of 0.15, and so there are four random variables in this case. As the results in Table 6 show, the computational errors of the mean value and the Std are very small. This demonstrates that the proposed method is reliable and can produce accurate results.

2. Robust Optimization of the HST Solar Array

The material parameters ε and α_s of the two booms are taken as design variables that are within the intervals of [0.1, 0.5] and [0.3, 0.8], respectively. The design objective is minimizing the maximum deflection of point A. The parameters ε and α_s with the CV of 0.05, and the two angles θ_1 and θ_2 in the interval of [−15°, 15°] are considered as random variables. The Hooke–Jeeves direct search method is adopted for optimization.

Fortunately, the mean value and the Std of the objective do not conflict with each other, and so they can reach the optimal results simultaneously (listed in Table 7). The table shows that both the mean value and the Std are greatly reduced after the optimization, which indicates a more robust design.

Table 4 Robust optimization results of the cantilever beam

	Initial value	Optimal results at Pareto front										
h, cm	2.54	1.639	1.856	1.942	2.011	2.073	2.132	2.178	2.247	2.306	2.354	3.246
b, cm	2.54	2.002	1.795	1.774	1.759	1.743	1.726	1.714	1.700	1.694	1.695	3.246
Mean w/L	0.594	0.913	0.898	0.888	0.879	0.869	0.859	0.850	0.835	0.820	0.806	0.263
Std w/L	0.093	0.010	0.015	0.020	0.025	0.030	0.035	0.039	0.045	0.050	0.055	0.057

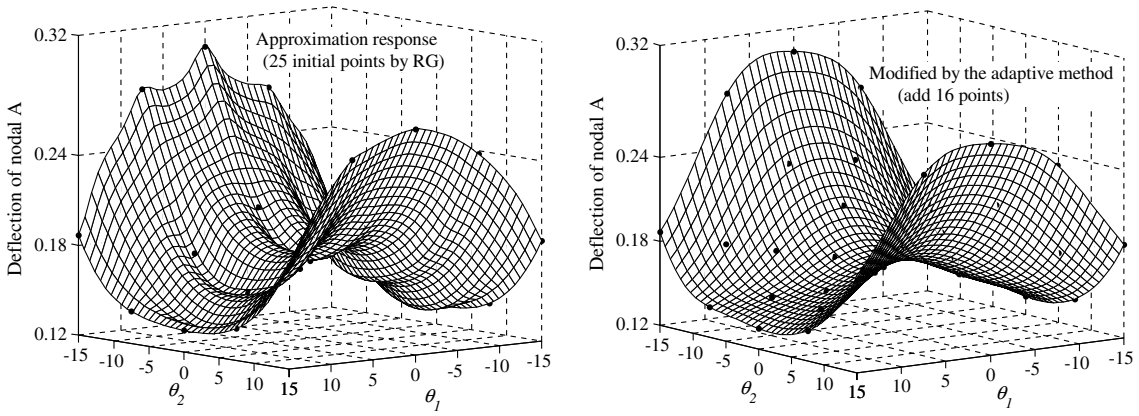

a) With the initial sampling points **b) With the final sampling points**

Fig. 8 Approximation response surface.

Table 5 Stochastic response of the maximum deflection of point A

		Kriging model (adaptive)	
	DMCS	RG Initial: 5×5 points, final: 41 points	TPLHD Initial: 16 points, final: 36 points
Mean value, m	0.1833	0.1840	0.1836
Absolute relative error, %	——	0.382	0.164
Std, m	0.0370	0.0374	0.0367
Absolute relative error, %	——	1.081	0.811
Computational time, Minutes	7240	297	261

Table 6 Stochastic response of the maximum deflection of point A

		Kriging model (adaptive)	
	DMCS	TPLHD	Initial: 16 points, final: 36 points
Mean value, m	0.1833	0.1829	
Absolute relative error, %	——	0.218	
Std, m	0.0449	0.0448	
Absolute relative error, %	——	0.223	

Table 7 Robust optimization results of the HST solar array

	Initial value	Optimal results
ε	0.130	0.467
α_s	0.500	0.343
Mean, m	0.186	0.120
Std, m	0.035	0.019

VII. Conclusions

This paper presents a robust design method for the complex LSSS subjected to incident heat flux and energy emission by radiation. First, an adaptive space estimation algorithm is proposed by using the kriging model. Based on this model, the stochastic responses of flexible LSSSs can be efficiently calculated by the MCS or the PSFEM instead of using the expensive thermal–dynamic coupling analysis repeatedly. Finally, a biobjective optimization problem that involves the mean value and the Std of structural response is formulated to consider the robustness of the design. The corresponding Pareto front is efficiently obtained by transforming this biobjective optimization problem into a single-objective optimization problem by adding an equality constraint.

Through numerical examples, it is demonstrated that the stochastic responses obtained by the MCS or the PSFEM based on the kriging model agree very well with those from the DMCS. The robust design scheme can be efficiently implemented for the design of complex LSSSs considering the thermal–dynamic coupling effect and geometric nonlinearity.

References

[1] Frisch, H. P., and Harold, P., "Thermally Induced Vibrations of Long Thin-Walled Cylinders of Open Section," *Journal of Spacecraft and Rockets*, Vol. 7, 1970, pp. 897– 905. doi:10.2514/3.30068

[2] Thornton, E. A., and Foster, R. S., "Dynamic Response of Rapidly Heated Space Structure," *Computational Nonlinear Mechanics in Aerospace Engineering*, Progress in Astronautics and Aeronautics, Vol. 146, AIAA, Washington, D.C., 1992, pp. 1185–1203.

[3] Thornton, E. A., and Kim, Y. K., "Thermally Induced Bending Vibrations of a Flexible Rolled-Up Solar Array," *Journal of Spacecraft and Rockets*, Vol. 30, No. 4, 1993, pp. 438–448. doi:10.2514/3.25550

[4] Boley, B. A., "Thermally Induced Vibrations of Beams," *Journal of the Aeronautical Sciences*, Vol. 23, No. 2, 1956, pp. 179–181.

[5] Augusti, G., "Instability of Struts Subject to Radiant Heat," *Meccanica*, Vol. 3, No. 3, 1968, pp. 167–176. doi:10.1007/BF02129249

[6] Xue, M. D., and Ding, Y., "Two Kind of Tube Elements for Transient Thermal-Structural Analysis of Large Space Structures," *International Journal for Numerical Methods in Engineering*, Vol. 59, 2004, pp. 1335–1353. doi:10.1002/nme.918

[7] Xue, M. D., Duan, J., and Xiang, Z. H., "Thermally Induced Bending-Torsion Coupling Vibration of Large Scale Structures," *Computational Mechanics*, Vol. 40, 2007, pp. 707–723. doi:10.1007/s00466-006-0134-x

[8] Duan, J., Xiang, Z. H., and Xue, M. D., "Thermal-Dynamic Coupling Analysis of Large Space Structures Considering Geometric Nonlinearity," *International Journal of Structural Stability and Dynamics*, Vol. 8, No. 4, 2008, pp. 569–596. doi:10.1142/S0219455408002806

[9] Thomas, A. Z., Michael, J. H., et al., "Needs and Opportunities for Uncertainty-based Multidisciplinary Design Methods for Aerospace Vehicles," NASA TM-2002-211462, 2002.

[10] Park, G. J., Lee, T. H., Lee, K. H., and Hwang, K. H., "Robust Design: An Overview," *AIAA Journal*, Vol. 44, No. 1, 2006, pp. 181–191. doi:10.2514/1.13639

[11] Schüeller, G. I., and Jensen, H. A., "Computational Methods in Optimization Considering Uncertainties—An Overview," *Computer Methods in Applied Mechanics and Engineering*, Vol. 198, 2008, pp. 2–13. doi:10.1016/j.cma.2008.05.004

[12] Simpson, T. W., Peplinski, J., Koch, P. N., and Allen, J. K., "On the Use of Statistics in Design and the Implications for Deterministic Computer Experiments," Proceedings of Design Theory and Methodology (DTM'97) ASME International, Paper DETC97/DTM-3881, 1997.

[13] Sobieszczanski-Sobieski, J., and Haftka, R. T., "Multidisciplinary Aerospace Design Optimization: Survey of Recent Developments," *Structural optimization*, Vol. 14, No. 1, 1997, pp. 1–23. doi:10.1007/BF01197554

[14] Koji, S., Jin, N. L., Jeong, S., Obayashi, S., and Koishi, M., "An Approach for Multi-Objective Robust Optimization Assisted By Response Surface Approximation and Visual Data-Mining," *2007 IEEE Congress on Evolutionary Computation, CEC 2007*, Inst. of Electrical and Electronics Engineers, Piscataway, NJ, pp. 2413–2420. doi:10.1109/CEC.2007.4424773

[15] Erwin, S., and Dick, D. H., "Robust Optimization Using Computer Experiments," *European Journal of Operational Research*, Vol. 191, No. 3, 2008, pp. 816–837. doi:10.1016/j.ejor.2007.03.048

[16] Lee, K. H., and Park, G. J., "A Global Robust Optimization Using Kriging Based Approximation Model," *JSME International Journal, Series C*, Vol. 49, No. 3, 2006, pp. 779–788. doi:10.1299/jsmec.49.779

[17] Jin, R., Du, X., and Chen, W., "The Use of Metamodeling Techniques for Optimization Under Uncertainty," *Structural and Multidisciplinary Optimization*, Vol. 25, No. 2, 2003, pp. 99–116. doi:10.1007/s00158-002-0277-0

[18] Sacks, J., Welch, W. J., Mitchell, T. J., and Wynn, H. P., "Design and Analysis of Computer Experiments," *Statistical Science*, Vol. 4, No. 4, 1989, pp. 409–435. doi:10.1214/ss/1177012413

[19] Viana1, F. A. C., Venter, G., and Balabanov, V., "An Algorithm for Fast Optimal Latin Hypercube Design of Experiments," *International Journal for Numerical Methods in Engineering*, Vol. 82, No. 2, 2010, pp. 135–156. doi:10.1002/nme.2750

[20] Liu, W. K., Belytschko, T., and Mani, A., "Random Field Finite Elements," *International Journal for Numerical Methods in Engineering*, Vol. 23, 1986, pp. 1831–1845. doi:10.1002/nme.1620231004

[21] Nocedal, J., and Wright, S. J., *Numerical Optimization*, 1st ed., Springer Science, New York, 1999.

P. Gage
Associate Editor